



Impact coefficient of reinforced concrete slab on a steel girder bridge

Kim, Chul-Woo
Kawatani, Mitsuo
Kwon, Young-Rog

(Citation)

Engineering Structures, 29(4):576-590

(Issue Date)

2007-04

(Resource Type)

journal article

(Version)

Accepted Manuscript

(URL)

<https://hdl.handle.net/20.500.14094/90000471>



Impact coefficient of reinforced concrete slab on a steel girder bridge

Chul-Woo Kim^{a,*}, Mitsuo Kawatani^a, Young-Rog Kwon^b

^a*Department of Civil Engineering, Kobe University, 1-1 Rokkodai, Nada, Kobe 657-8501, Japan*

^b*Department of Civil Engineering, Dong-A University, 840 Hadan2, Saha, Busan 604-714, Korea*

Abstract

Impact coefficients of reinforced concrete slabs on a steel girder bridge are simulated using a three-dimensional traffic-induced dynamic response analysis of bridges combined with the Monte Carlo simulation technique. This paper presents examination of the effect of the impact coefficient on fatigue performance of RC slabs. Results show that surface roughness is the most influential factor of the RC slab's impact coefficient. The bump height is another important factor for the slab located near the bump along with the surface roughness. It is also observed that the slab near the expansion joint of the approaching side of the bridge shows the greatest impact coefficient. However, even though the slab near the expansion joint experiences the most severe dynamic loading effect, the slab located near the expansion joint, which is rendered stronger by its deeper cross section, has a lower probability of fatigue failure than other panels. The parametric study shows that the probability of the fatigue failure tends to increase with decreasing concrete quality. It can be concluded that a code-specified impact coefficient leads to a conservative fatigue design for RC slabs of well maintained highway bridges. In contrast, the higher impact coefficient resulting from the worse roadway surface condition and higher traffic speed can hasten wear and cause premature fatigue failure of RC slabs.

Keywords: Impact coefficient; RC slab; Fatigue; Traffic-induced vibration; Monte Carlo Simulation; Probability of failure

1. Introduction

A reinforced concrete (RC) slab that is directly subjected to wheel loads is the most important structural element in distributing wheel loads of vehicles. Deterioration in the RC slab may cause distress in the girders and secondary load path elements such as diaphragms. A rational criterion for performance of the slab thus provides a useful assessment tool for decision-making in relation to bridge management because the maintenance, rehabilitation and replacement of the slab comprise a large fraction of the bridge's life-cycle cost [1]. Japan's Ministry of Land,

* Corresponding author

Phone: +81-78-803-6383, Fax: +81-78-803-6069, e-mail: cwkim@kobe-u.ac.jp

Infrastructure and Transportation has determined that about 67% of the need for steel bridge reconstruction in Japan is attributable to damage to RC slabs [2].

The average life of an RC slab is determined by many factors including initial design, material properties, traffic, environment, salt application, presence and effectiveness of protective systems, and maintenance practices [3]. All of those factors influence crack development in RC slabs during their service [4]. Cracking in RC slabs reduces the load capacity and hastens fatigue failure [5, 6, 7]. Fatigue of the RC slab is caused by the total moving wheel load of static truck loads and dynamic load effects from roadway roughness, dynamic properties of vehicles, vehicle speeds, and others. The bump near expansion joints is another important factor for the slab because of the impulsive loading effect by vehicles passing over the bump [8, 9]. Generally in bridge design, dynamic load effects exerted by moving vehicles on bridges and RC slabs are considered using the impact coefficient.

Vehicle motion induced by surface roughness of bridges with bumps will stimulate the slab as well as the entire bridge system. It is not deterministic, but rather stochastic or purely random. The vehicle speed, the axle weight of vehicles and the traveling position of vehicles also affect dynamic responses of bridges as random variables in addition to the roadway roughness.

A fatigue test for RC slabs by Matsui [10] shows that the equivalent loading cycles is proportional to the load ratio raised to the twelfth power (see Eq. (11) in section 5.1). The test indicates that the axle load, including the impact coefficient raised to the twelfth power, affects the RC slab fatigue performance. However, only the probability distribution of axle loads is considered in fatigue assessment and design of the RC slab. In contrast, the worst case scenario is considered in the code-specified impact coefficient because of deficient data. This conservative approach is acceptable for the design of new structures. For existing structures, however, it may lead to unnecessary and costly strengthening. Another important point to be examined is whether the code-specified impact coefficient for slabs provides a conservative design for RC slabs or not.

Better understanding of the RC slab's impact coefficient is crucially important to elucidate the deterioration process of RC slabs, including fatigue. However most of the previous works to date have focused on dynamic responses of bridge girders [e.g. 11-14]. Even though Broquet et al. [15] report the dynamic amplification factor of deck slabs of concrete road bridges through a numerical investigation, information regarding the impact coefficient of RC slabs and effects of dynamic interaction between the slab and the axle load remains insufficient despite the importance of that information for determining the fatigue strength of the RC slab.

This study is intended to outline the features of the impact coefficient of RC slabs based on a probabilistic approach. We clarify the effect of the impact coefficient on the fatigue performance of RC slabs. A three-dimensional (3D) traffic-induced dynamic response analysis of

bridges [14] is used to simulate the impact coefficient for RC slabs along with the Monte Carlo simulation (MCS) technique. The simulation incorporates randomness of the surface roughness of bridges, the bump height, the vehicles' traveling positions, the vehicles' axle weights, and vehicle speed.

2. Analytical procedure

Finite element (FE) method is used for modal analysis as a tool for idealizing bridges for dynamic response analysis. A consistent mass system and Rayleigh damping are respectively adopted to form mass and damping matrices of a bridge model. The authors' previous works [14, 16-17] present details of the analytical procedure.

Two types of finite elements are adopted to idealize members of the bridge superstructure. A beam element, with six degrees-of-freedom (DOFs) at each node, is used to idealize girders, crossbeams and guardrails. A flat shell element with four nodes [18] is adopted for the slab. Uncracked sections are assumed for RC deck slabs. Static reduction introduced by Guyan [19] is performed to improve the calculation efficiency: the vertical deflection is taken as the master DOF, which is retained because no external force acts on the bridge except in the vertical direction.

Matrix formation of the forced vibration of a bridge system under moving vehicles can be defined as shown in Eq. (1) [14],

$$\begin{bmatrix} \mathbf{M}_{bb} & \mathbf{0} \\ \mathbf{Sym.} & \mathbf{M}_{vv} \end{bmatrix} \begin{Bmatrix} \ddot{\mathbf{a}} \\ \ddot{\mathbf{Z}} \end{Bmatrix} + \begin{bmatrix} \mathbf{C}_{bb} & \mathbf{C}_{bv} \\ \mathbf{Sym.} & \mathbf{C}_{vv} \end{bmatrix} \begin{Bmatrix} \dot{\mathbf{a}} \\ \dot{\mathbf{Z}} \end{Bmatrix} + \begin{bmatrix} \mathbf{K}_{bb} & \mathbf{K}_{bv} \\ \mathbf{Sym.} & \mathbf{K}_{vv} \end{bmatrix} \begin{Bmatrix} \mathbf{a} \\ \mathbf{Z} \end{Bmatrix} = \begin{Bmatrix} \mathbf{f}_{bb} \\ \mathbf{f}_{vv} \end{Bmatrix}, \quad (1)$$

where \mathbf{M} , \mathbf{C} and \mathbf{K} respectively indicate the mass, damping and stiffness matrices of a system, \mathbf{a} and \mathbf{Z} respectively represent the displacement vectors of the bridge and vehicle; and \mathbf{f} is the interaction force vector. Subscripts bb , vv and bv denote the bridge, vehicle and bridge-vehicle interaction, respectively, and (\cdot) represents the derivative with respect to time.

An alternative step-by-step solution using Newmark's β method [20] is applied to solve the derived system of governing equations of motion. The value of 0.25 is used for β . Solutions are obtainable within a less than 0.001 relative margin of error.

A simplified algorithm for a traffic-induced vibration analysis of a bridge is shown in Figs. 1 and 2. It includes the process of considering the randomness of influencing factors to dynamic responses of a bridge. For estimating the impact coefficient, in this paper the dynamic increment has been determined in accordance with EMPA's procedure [21] as shown in Fig. 3 and Eq. (2).

$$i = \frac{M_{dy,max} - M_{st,max}}{M_{st,max}}, \quad (2)$$

where, $M_{dy,max}$ is the maximum bending moment at the observation position under dynamic vehicular loadings and $M_{st,max}$ is the bending maximum moment at the observation position under static vehicular loadings.

The simplified algorithm is as follows [14, 16];

1. Form the mass and stiffness matrices of the bridge: M_{bb} and K_{bb} .
2. Eigen value analysis: natural frequencies and natural modes
3. Build the damping matrix of the bridge by Rayleigh damping: C_{bb} .
4. Normalize the equations of motion of the bridge.
5. Determine the longitudinal position of each tire of the vehicle on the bridge; Set initial conditions of the displacement, velocity and acceleration for each degree-of-freedom of the vehicle and bridge.
6. Start the iterative process (see Fig. 2);

Step1: Assume accelerations of the vehicle and bridge at the time $t+\Delta t$; Calculate new wheel positions of the vehicle at the time $t+\Delta t$ under the traveling speed of v ; At each wheel position, the roadway profile and bridge deflection are computed; The displacement and velocity at each mass of the vehicle model are calculated; Modal displacements and velocities of the bridge are computed

Step2: Calculate the displacements and velocities of the bridge by back transforming the modal responses in terms of a linear combination of the eigen functions; Compute the modal force of the bridge; Equations of motion of the bridge are solved to obtain the modal accelerations; Calculate the dynamic wheel load at each wheel; The equations of motion for the vehicle are solved to obtain acceleration.

Step 3: Check tolerances.

The above process from Step1 to Step3 is repeated until the tolerance is satisfied.

7. The impact coefficients (see Eq. (2)) [21] of decks are estimated and saved, if a vehicle passes the bridge completely.
8. Repeat the above process from 5 to 7 until the repeated number reaches a certain number of samples.

3. Model description

3.1. Bridge model

The bridge considered in this study is a simple-span composite steel-plate girder bridge. Figure 4 shows that it comprises three girders with a span length of 40.4 m. As for RC slabs, the slab thickness at the approaching side is 23 cm thick. That at the middle section is 17 cm thick and the span length is 2.65 m. The slab is assumed to act compositely with main girders. Table 1 presents a summary of the bridge characteristics. Figure 4(c) shows observation points denoted as P1, P2, P3, P4 and P5. The panel where point P1 is located has 23 cm thickness. The other panels have 17 cm thickness. Figure 5 shows cross sections of RC slabs of the bridge. The FE model consists of 570 nodes. The bridge's dynamic response is estimated by superposing the modes up to the 246th mode (494 Hz) because the slab's dynamic response is sufficiently converged within the mode from a preliminary investigation. The 246th mode is the fifth bending mode of the RC slab.

Fundamental frequencies of bending and torsion modes taken from eigenvalue analysis are calibrated to coincide with those obtained from a field test. The validity of the analytical responses of RC slabs was verified through comparison with field-test data [9, 22]. A part of time histories of decks taken from the experiment and analysis is shown in Fig. 6, in which measured roadway profiles of the bridge are used in analysis. Observations from the dynamic responses of decks in Fig. 6 demonstrate that the quality of agreement between the experimental and analytical results is quite acceptable in light of the potential sources of error.

3.2. Vehicle model

Traffic including a high proportion of heavy trucks on highway bridges usually occurs at night. The maximum traffic constitution among heavy trucks has been reported as three-axle vehicles in Japan [23]. Therefore, a dump truck with a tandem axle idealized as an eight-degree-of-freedom model (see Fig. 7) is adopted as a vehicle model. Table 2 presents a summary of vehicle model properties. Validity of the vehicle model for the traffic-induced dynamic response analysis of bridges was verified through comparison to experimental data. A detailed summary of the validation and experiment is available in another work [14]. Vehicles are assumed to move from the left to the right end of the bridge.

3.3. Random variables

3.3.1 Roadway profile

Fluctuation of the roadway surface can be treated as a homogeneous Gaussian random process with zero mean [24]. The probability can be defined as a power spectral density (PSD) function. The following analytical description has been proposed to fit the measured PSD [25].

$$S(\Omega) = \alpha / (\Omega^n + \beta^n), \quad (3)$$

where $\Omega (= \omega/2\pi)$ is the space frequency (cycle/m) and α , β and n are the roughness coefficient, shape parameter and parameter to express the distribution of power of the PSD curve, respectively; ω represents the circular frequency of the road surface.

Regarding parameters in Eq. (3), $\alpha=0.001$, $\beta=0.05$ and $n=2.0$ are used in this study based on measured data of Meishin Expressway, which links Nagoya with Kobe in Japan, before service. The PSD curve, with $\alpha=0.003$, $\beta=0.05$ and $n=2.0$, is also considered in order to investigate the effect of roadway surface conditions on the impact coefficient of RC slabs. The PSD curves are shown in Fig. 8 with ISO estimates [26], in which paved roads are considered to be among road classes A–D, whereas the road classes E and F correspond to unpaved roads on which a truck can hardly travel at 40 km/h.

Roadway profile samples are obtainable using MCS method based on the sampling function expressed as Eq. (4) if a PSD function for a roadway profile is defined.

$$z_r(x) = \sum_{k=1}^M a_k \sin(\omega_k \cdot x + \varphi_k), \quad (4)$$

where the a_k is a Gaussian random variable with zero mean and variance $\sigma_k^2 = 4S(\omega_k)\Delta\omega$, the φ_k is a random variable having uniform distribution between 0 and 2π . In addition, ω_k is the circular frequency of roadway surface roughness written as $\omega_k = \omega_L + (k-1/2)\Delta\omega$, $\Delta\omega = (\omega_U - \omega_L)/M$. The upper and lower limits of the frequency are respectively designated as ω_U and ω_L , and M is a sufficiently large integer number; $S(\omega_k)$ is the PSD of a roadway profile.

3.3.2 Bump height near expansion joints

The lognormal distribution is selected to describe the probability distribution of bump heights at expansion joints of bridges based on survey results of national roadway bridges in Japan [27]. Among the measured bump profiles, the sine-shaped bump profile that gives the most severe effect on the impact coefficient of decks from a preliminary study is adopted in the simulation. The respective mean value and standard deviation of the measured bump heights were 20.4 mm and 7.0 mm [27]; the sine wave length of the bump profile in the driving direction is assumed as 100 cm. The highway bridges' pavement is generally better maintained than that of

national roadway bridges. Consequently, half of the measured height is also considered in the simulation. The measured bump height on national roadway bridges is also used in the simulation to investigate the effect of bump height on the impact coefficient of the RC slab. The bump location considered in this study is on the bridge expansion joint.

3.3.3 Traffic data

The vehicles' impulsive loading effect that is generated during vehicles' passage over a bump near an expansion joint can travel further from the expansion joint with increasing speed. Thus, the vehicle speed is considered as a random variable. The travelling position of vehicles is also considered as a random variable. A normal distribution is assumed for the travelling speed and position of vehicles on highway bridges based on the Hanshin Expressway database. Even though today's traffic environment shows a tendency toward increase in the travelling speed, the mean value and standard deviation of vehicle speeds are assumed respectively as 70 km/h and 10 km/h according to the previous research [23]. To simulate the impact coefficient of RC slabs on national roadway bridges, a vehicle speed model with respective mean and standard deviation values of 50 km/h and 10 km/h is used in the analysis. The mean value and standard deviation for the travelling positions of vehicles are 0.0 m and 0.2 m from a target passage [28].

A lognormal distribution is assumed for the axle load of the three-axle vehicles according to the Hanshin Expressway measured data. The mean value and standard deviation of the axle load are 49.805 kN and 12.056 kN respectively for the front axle, 90.507 kN and 34.276 kN for the front wheel of the tandem axle, and 67.571 kN and 31.637 kN for the rear wheel of the tandem axle [28].

4. Simulation of the impact coefficient

A number of sample roadway profiles, bump heights, vehicle speeds, travelling positions of vehicles, and axle loads are generated using the MCS technique. A 3D dynamic response analysis of the steel plate girder bridge with moving vehicles is conducted to estimate the impact coefficient of the panels according to each sample of random variables.

This study creates four scenarios that illustrate how the impact coefficient changes based on different roadway surface condition and traffic speed. The scenarios are as follows:

Scenario 1 (SCN-1): the roadway profile with $\alpha=0.001$, $\beta=0.05$ and $n=2.0$ as parameters of the PSD function defined in Eq. (3); bump heights' mean and standard deviation values are 10.2 mm and 3.5 mm, respectively; mean and standard deviation values of the vehicle speed are 70 km/h and 10 km/h, respectively.

Scenario 2 (SCN-2): the roadway profile with $\alpha=0.001$, $\beta=0.05$ and $n=2.0$ as parameters of the PSD function defined in Eq. (3); bump heights' mean and standard deviation values are 20.4 mm and 7.0 mm, respectively; mean and standard deviation values of the vehicle speed are 70 km/h and 10 km/h, respectively.

Scenario 3 (SCN-3): the roadway profile with $\alpha=0.003$, $\beta=0.05$ and $n=2.0$ as parameters of the PSD function defined in Eq. (3); bump heights' mean and standard deviation values are 20.4 mm and 7.0 mm, respectively; mean and standard deviation values of the vehicle speed are 50 km/h and 10 km/h, respectively.

Scenario 4 (SCN-4): the roadway profile with $\alpha=0.003$, $\beta=0.05$ and $n=2.0$ as parameters of the PSD function defined in Eq. (3); bump heights' mean and standard deviation values are 20.4 mm and 7.0 mm, respectively; mean and standard deviation values of the vehicle speed are 70 km/h and 10 km/h, respectively.

The scenario SCN-1 assumes a situation of highway bridges, whereas the SCN-3 is for national roadway bridges. Scenario SCN-2 is adopted to investigate the effect of the bump height on the impact coefficient of RC slabs of highway bridges. Scenario SCN-4 is adopted to investigate the effect of the vehicle speed on the impact coefficient of RC slabs on national roadway bridges. The four scenarios consider the same data of the travelling position and axle load described in section 3.3.3.

Three hundred samples of each random variable are taken into account to simulate the impact coefficient considering all the random variables to save computation time because a preliminary investigation demonstrates that the mean and standard deviation values of the simulated impact coefficient tend to converge within the 300 samples (see Fig. 9). No correlation is assumed among the random variables described in section 3.3.

The approximately straight lines on the lognormal probability paper of Fig. 10 suggest that the simulated impact coefficient of the RC slab can be characterized as the lognormal distribution. The impact coefficients obtained by simulation are shown in Table 3, which also provides the simulated impact coefficient of an external girder (specified as G1 in Table 3) at the span center.

4.1. Effect of random variables to the impact coefficient of RC slabs

The effect of each random variable on the impact coefficient of the RC slab is shown in Fig. 11 using the reliability index, which is calculated from Eq (5).

$$\beta = \frac{\ln(i_{code}) - \mu_{\ln(i)}}{\sigma_{\ln(i)}}, \quad (5)$$

where β is the reliability index; i_{code} is the impact factor specified in the code of Japan Road Association (JRA) (see Eq. 6); i is the simulated impact factor; $\mu_{\ln(i)}$ is the mean value of $\ln(i)$; and $\sigma_{\ln(i)}$ is the standard deviation of $\ln(i)$.

$$i_{code} = 20 / (L + 50), \quad (6)$$

where L is the span length of the RC slab in meter; for the bridge model, $L = 2.65$ m and i_{code} becomes 0.380.

The most influential factor on the impact coefficient of the RC slab is found to be the surface roughness from Fig. 11, which shows the effect of each random variable on the impact coefficient of each panel of the RC slab. An interesting point that is apparent from Fig. 11 is that, in addition to the surface roughness, the bump height is an important factor for the impact coefficient of the P1 panel located near the bump. Moreover, the combination of all random variables, as in SCN-1 in the simulation of the impact coefficient, also shifts the reliability index of the P1 panel to the lowest value because of the effect of the bump on the dynamic response of the P1 panel. It indicates that the P1 panel experiences more severe dynamic loading effects than the other panels do.

4.2. Impact coefficients according to each scenario

The reliability of the impact coefficients specified in the JRA code according to each scenario (SCN-1 to SCN-4) is investigated to show how the impact coefficient changes based on the different roadway surface condition and traffic speed.

The reliability index is shown in Fig. 12 with the limit states defined in the Eurocode One. The target reliability indices (β_i) proposed in the Eurocode are 1.5 for the serviceability limit state (SLS), 3.8 for the ultimate limit state (ULS), and 1.5–3.8 for the fatigue limit state (FLS). The kind of limit state into which the impact coefficient is classified has not been defined yet.

Comparing SCN-3 for national roadway bridges with SCN-1 for highway bridges shows that the slab on national roadway bridges experiences more severe dynamic load effect than highway bridges as expected. Interesting points in Fig. 12 include the effects of bump and traffic speed on the RC slab impact coefficient: comparison of SCN-2 with SCN-1 again suggests that the bump is an influential factor on dynamic responses of the RC slab near the bump, such as the P1 panel; regarding the effect of the traffic speed, comparison of the reliability index of SCN-3 with SCN-4 with a faster traffic speed than that of SCN-3 shows that the traffic speed strongly affects the slab's dynamic responses. The impulsive wheel load generated as the vehicle passes over the bump can travel further with increasing speed. Consequently, the panel located distant from the bump can be affected by the impulsive loading. Observations reveal that

traffic speed is another important factor that should be used to assess the impact coefficient of RC slabs.

5. Application of the simulated impact coefficient for RC slab fatigue

Simulation of the impact coefficient of RC slabs demonstrates that the traffic-induced dynamic response of the P1 panel located at the approaching side of the bridge is greater than that of other panels because of the bumps at expansion joints. Generally, design codes specify that the panel near expansion joints should be stronger than other panels. A question here is whether or not the severe wheel load affects fatigue performance of the RC slab located near an expansion joint. A simple reliability analysis for fatigue performance of the RC slab shown in Fig. 5 is conducted to answer that question. Investigations specifically address the effect of the impact coefficient on fatigue performance of the RC slab as a numerical example. The fatigue performance of the RC slab is estimated using the probability of fatigue failure for a given lifetime. In this study, the RC slab lifetime is assumed as 100 years. The fatigue failure probability is estimated by comparing the punching shear strength of the RC slab and traffic load effects over the 100-year lifetime.

Traffic data are the same as those described in section 3.3.3. For the impact coefficient with lognormal distribution, the mean and standard deviation values summarized in Table 3 are used. The average daily truck traffic (ADTT) is assumed as 10,000 vehicles. Table 4 lists properties of concrete and reinforcing bars of RC slabs used in reliability analysis to assess the fatigue performance of the RC slab. The MCS is conducted to estimate the RC slab's probability of fatigue failure.

5.1. Performance function for fatigue of RC slabs

Previous researches in relation to the fatigue of the RC deck slabs using a moving pulsating load [29] and simulated moving wheel load [28, 30, 31] on deck models suggest following fatigue failure process. By the actions of compression and twisting at the faces of the crack of RC deck slabs due to moving loads the crack faces wear away. In addition to opening and closing of cracks, there is sliding up and down of the crack interfaces. Cracks then grow because of load cycles and cause further deterioration. After that instant, existing cracks propagate through the thickness, instead of forming new cracks. Before yielding of reinforcement, the debonding along the bottom reinforcement, so called shear punching failure, occurs.

In this study, thereby, spalling of concrete with holes punched through the deck before yielding of reinforcement is assumed as the fatigue failure mode of the RC deck, because, at this

stage of deterioration, the serviceability of the deck is so impaired that a decision on rehabilitation, or repair should be taken [29].

The performance function for fatigue of RC slabs is

$$g(R, S) = R - S, \quad (7)$$

where R and S respectively represent the load-carrying capacity of an RC slab and the load effect. The failure probability is obtainable by counting the total events of $g < 0$ during a given life-time.

The punching shear strength (P_{sx}) of an RC slab, which can be estimated using Eq. (8) [30, 32], is adopted as the load-carrying capacity of the RC slab:

$$R = P_{sx} = 2B(f_{smax}x_m + f_{tmax}C_m), \quad (8)$$

where B is the effective width of fatigue failure of RC decks ($B=b+2D_d$), b is the contact width of the loading plate or tire in the direction of distribution bars, D_d is the effective depth of distribution bars, f_{smax} is the maximum shear stress of concrete ($f_{smax}=0.252f_{ck} - 0.000246f_{ck}^2$), f_{ck} is the compressive strength of concrete, f_{tmax} is the maximum tensile stress of concrete ($f_{tmax}=0.583f_{ck}^{2/3}$), x_m is the distance between the neutral axis and the edge of compression part of the main section, and C_m is the depth of concrete covering the main section.

A relationship between the load effect and the number of loading cycles can be expressed as the following equation [10, 28, 30] of the Miner's rule based on the S-N curve for RC slabs taken from a moving wheel load test, and Perdikaris et.al. [31] suggest a similar formulation.

$$\text{Log}(P/P_{sx}) = -k \text{Log} N + \text{Log} C = -0.07835 \text{Log} N + \text{Log} 1.52, \quad (9)$$

where P is the wheel load and N is the total number of loading cycles ($N=N_{eq} \times$ fatigue life in year) caused by P , and the N_{eq} is the equivalent loading cycle defined in Eq. (13).

If an RC slab undergoes fatigue failure under N_0 loading cycles of a load P_0 and N_1 cycles of a load P_1 , then the relation between the load and loading cycles is as shown below.

$$\text{Log}(P_0/P_{sx}) = -k \text{Log} N_0 + \text{Log} C \quad (10-1)$$

$$\text{Log}(P_1/P_{sx}) = -k \text{Log} N_1 + \text{Log} C \quad (10-2)$$

Equations (10-1) and (10-2) provide the relation as

$$N_0 = (P_1/P_0)^{1/k} \times N_1 = (P_1/P_0)^m \times N_1, \quad (11)$$

where $m = k^{-1} = 1/0.07835 = 12.76$.

Equation 10 shows that the relation in Eq. (11) can be expanded to consider an actual traffic condition such as load P_1 of N_1 cycles, P_2 of N_2 cycles, ... and P_n of N_n cycles.

$$N_0 = \int_0^{P_{\max}} (P/P_0)^m \cdot f(P) \cdot dP \times N_i \quad (12)$$

The equivalent loading cycle for a standard load P_0 considering randomness of the axle load and impact coefficient can be defined as Eq. (13) [28].

$$N_{eq} = \int_0^{i_{\max}} \int_0^{P_{\max}} \{\kappa \cdot (1+i) \cdot (P/P_0)\}^m f(i) \cdot f(P) \cdot dP \cdot di \times N_i \quad (13)$$

In that equation, N_{eq} is the equivalent loading cycle corresponding to a standard wheel load P_0 ; κ is a deviation factor to consider the difference between the wheel load effect under a real traffic condition and the load effect during the fatigue test of RC slabs; i represents the impact coefficient; N_i indicates total loading cycles of an axle load per year; P is the random axle load; $f(i)$ denotes the probability density function of impact coefficients; and $f(P)$ is the probability density function of axle loads.

To simplify the numerical example, κ in Eq. (13) is estimated by assuming that the probability of fatigue failure of the RC slab at the middle section of the bridge is 100% within a hundred years (the given life time) under consideration of the deterministic impact coefficient of 0.38 specified in the JRA code, even though the deviation factor should be determined precisely using FE method. In other words, using the estimated κ indicates that the slab is designed to have a fatigue life of 100 years by considering the code-specified impact coefficient. Next, the equivalent loading cycle N_{eq} for a standard load P_0 is calculated considering randomness of the impact coefficient according to Eq. (13). The P_{sx} taken from Eq. (9) by substituting the N_{eq} estimated from Eq. (13) illustrates the load effect on the RC slab. The load-carrying capacity of the RC slab is calculated by considering the normal distribution of the compressive strength of concrete f_{ck} in Eq. (8). Equation (7) gives the final probability of fatigue failure of each slab in a given fatigue life span. The standard wheel load P_0 is set as 9.81 kN.

5.2. Effect of the impact coefficient on fatigue performance of RC slabs

The fatigue performance of each panel according to the simulated impact coefficient is investigated next. As described in section 5.1, the RC slab is assumed to have a design fatigue life of a hundred years under the impact coefficient of 0.38 according to the JRA code. The probability of fatigue failure of each panel within the design fatigue life considering the simulated impact coefficients according to respective scenarios is summarized in Figs. 13–16.

The P1 panel located near the expansion joint usually adopts a deeper cross-section and more reinforcing bars to resist the expected severe wheel load effects. However, congested areas containing much reinforcing steel may engender poor concrete quality because of rock pockets and sand streaks that result from the difficulty of placing concrete. Therefore, to consider the

situation of poor concrete quality for the P1 panel, the ninetieth and eightieth percentiles of the compressive strength of concrete are also considered in this investigation. The $R(f_{ck})$, $R(0.9f_{ck})$ and $R(0.8f_{ck})$ in Figs. 13, 14, 15 and 16 respectively demonstrate the load carrying capacity of the RC slab taken from considering full, ninetieth and eightieth percentiles of the concrete strength.

Regarding SCN-1 (see Fig. 13), which denotes the scenario for general highway bridges, the probability of fatigue failure of the P1 panel distributed between 11.7% and 51.1% with respect to the concrete strength of the P1 panel, whereas those probabilities of other panels, especially P2 and P3 panels, are 96.3% and 95.4%, respectively. It indicates that the code-specified impact coefficient can provide a conservative design for fatigue of RC slabs because the failure probability is set as 100% under the code-specified impact coefficient.

The change in fatigue performance attributable to the increasing bump height of the highway bridge is determined by considering SCN-2. Comparison of Fig. 14(a) with Fig. 13(a) illustrates that the increase of bump height markedly affects the fatigue performance of the P1 panel. Moreover, comparison of the fatigue performance shown in Fig. 14(b) of SCN-2 with that of SCN-1 in Fig. 13(b) shows that the fatigue performance of the P2 panel is affected by the increase of the bump height, whereas the probability of fatigue failure of the P3 panel does not show great change. It demonstrates that the increase of a bump can affect even distant parts of the slab.

The situation for national roadway bridges of Japan, as illustrated in SCN-3, is also examined and summarized in Fig. 15. It has worse roadway surface conditions and lower traffic speeds than highway bridges resembling SCN-1. The fatigue performance of the RC slab according to SCN-4, which adopts a higher speed than SCN-3, is shown in Fig. 16. The fatigue life of a panel located distant from the bump dramatically decreases according to increased speed. One reason may be that the impulsive energy of vehicles resulting from impact with the bump travels further according to the traffic speed despite the large damping of the vehicle.

Observations from Fig. 13 to Fig. 16 show that the failure probability of the P1 panel is lower in comparison with other panels because of the deeper cross-section, even though the P1 panel experiences greater dynamic effects than other panels, as shown in Fig. 12. On the other hand, the probability of fatigue failure tends to increase with decreasing concrete quality. In particular, Figs. 14 and 15 show that the eightieth percentile of the concrete strength raises the failure probability of the P1 panel to a level that is equal to or higher than that of other panels. Based on these observations, it can be concluded that the code-specified impact coefficient may lead to a conservative fatigue design for RC decks for well-maintained highway bridges. However, the increase of the impact coefficient as a result of the worse roadway surface conditions and traffic speed may cause fatigue failure of RC slabs earlier than the design life.

6. Concluding remarks

Impact coefficients of the RC slab on a steel girder bridge were simulated in this study using 3D traffic-induced dynamic response analysis of bridges combined with the Monte Carlo simulation technique. The respective effects of each random variable on the impact coefficient of the RC slab were investigated. Reliability analysis using the fatigue limit state based on the existing experimental result was also conducted to assess the influence of the impact coefficient on the probability of failure resulting from fatigue.

The mean and standard deviation values of the simulated impact coefficient tend to converge within the 300 samples of random variables. The approximately straight lines shown on lognormal paper suggest that the simulated impact coefficient of the RC slab can be characterized by a lognormal distribution. The most influential factor on the impact coefficient of the RC slab is the surface roughness. Bump height, in addition to surface roughness, is another important factor for the impact coefficient of the P1 panel located near the bump. The combination of all the random variables in simulation of the impact coefficient also shifts the reliability index of the P1 panel to the lowest value, indicating that the P1 panel experiences more severe dynamic loading effect than that of other panels. The major point to be clarified is that, if the impact coefficient of the RC slab near the expansion joint of the approaching side of bridges satisfies a given reliability because of vehicles running on bumps, those reliabilities of other decks are satisfied automatically.

This study also demonstrates that the probability of the P1 panel's fatigue failure is lower than that of the other panels located at the bridge's middle section, even though the P1 panel experiences more severe dynamic loading effect than that of other panels. The probability is lower because of the higher strength of the P1 panel resulting from the deeper cross section. However, this study suggests that the probability of the fatigue failure of the P1 panel tends to increase with decreasing concrete quality.

Based on those observations, it can be concluded that the code-specified impact coefficient may lead to a conservative fatigue design for RC slabs for well maintained highway bridges. However the increased impact coefficient resulting from the worse roadway surface conditions and traffic speeds may cause fatigue failure of RC slabs earlier than the design life.

Results of this study demonstrate the importance of the impact coefficient of RC slabs through analytical approaches. A collection of impact coefficients of RC slabs is necessary to create a rational criterion for the slab performance level and decision-making in relation to bridge management.

References

- [1] Furuta H, Tsukiyama I, Dogaki M, Frangopol DM. 2003. Maintenance support system of steel bridges based on life cycle cost and performance evaluation. Reliability and optimization of structural systems. In: Furuta H, Dogaki M, Sakano M, Editors. Reliability and Optimization of Structural Systems. Swets & Zeitlinger Publishers; 2003, p. 205-13.
- [2] Public Work Research Institute. Results of survey on replacement of existing bridges. Technical Memorandum of PWRI, No.3512, Public Works Research Institute, Japan, 1997. (in Japanese)
- [3] Itoh Y, Kitagawa T. Using CO2 emission quantities in bridge lifecycle analysis, Engineering Structures, 2003; 25:565-77.
- [4] Zhang J, Li VC, Wu C. Influence of reinforcing bars on shrinkage stresses in concrete slab. Journal of Engineering Mechanics, ASCE 2000; 126(12):1297-300.
- [5] Matsui S. Technology developments for bridge decks-Innovations on durability and construction. Bridge and Foundation Engineering 1997; 8: 84-92. (in Japanese)
- [6] Perdikaris PC, Beim S. RC bridge decks under pulsating and moving load. Journal of Structural Engineering, ASCE 1988;114(3):591-607.
- [7] Kumar SV, GangaRao HVS. Fatigue response of concrete decks reinforced with FRP rebars. Journal of Structural Engineering, ASCE 1998;124(1):11-6.
- [8] Abe T, Sawano T, Kida T, Hoshino M, Kato K. Flexural load-carrying capacity and dynamic effects of RC beam due to running vibration load. Material Science Research International 2000;6(2):96-103.
- [9] Kawatani M, Kim CW. Effects of gap at expansion joint on traffic-induced vibration of highway bridge. Proceedings of Developments in Short and Medium Span Bridge Engineering'98, Calgary, Canada, July, 1998. CSCE [CD-ROM].
- [10] Matsui S. Study about fatigue of RC slab of highway bridges and design method. Doctoral thesis, Osaka University, 1984. (in Japanese)
- [11] Green MF, Cebon D. Dynamic response of highway bridges to heavy vehicle loads: Theory and experimental validation. Journal of Sound and Vibration 1994; 170(1): 51-78.
- [12] Wang TL, Huang D, Shahawy M, Huang K. Dynamic response of highway girder bridges. Computers and Structures 1996; 60(6): 1021-27.
- [13] Henchi K, Farfard M, Talbot M, Dhatt G. An efficient algorithm for dynamic analysis of bridges under moving vehicles using a coupled modal and physical components approach. Journal of Sound and Vibration 1998; 212(4): 663-83.
- [14] Kim CW, Kawatani M, Kim KB. Three-dimensional dynamic analysis for bridge-vehicle interaction with roadway roughness. Computers and Structures 2005; 83(19-20): 1627-1645.
- [15] Broquet C, Bailey SF, Fafard M, Brühwiler E. Dynamic behavior of deck slabs of concrete road bridges. Journal of Bridge Engineering, ASCE 2004; 9(2): 137-46.
- [16] Kim CW, Kawatani M, Hwang WS. Reduction of traffic-induced vibration of two-girder steel bridge seated on elastomeric bearings. Engineering Structures, 2004; 26(14):2185-95.

- [17] Kawatani M, Kim CW, Kawada N. Three-dimensional finite element analysis for traffic-induced vibration of steel two-girder bridge with elastomeric bearings. TRR, Journal of the Transportation Research Board 2005; CD 11-S: 225-33.
- [18] Zienkiewicz OC, Taylor RL. The finite element method, Vol.2, 5th ed. Butterworth-Heinemann, Oxford; 2000.
- [19] Guyan RJ. Reduction of stiffness and mass matrices. AIAA J 1965; 3(2): 380.
- [20] Newmark NM. A method of computation for structural dynamics. Journal of Engineering Mechanics Division, ASCE 1970; 96: 593-620.
- [21] Catieni R. Dynamic behavior of highway bridges under passage of heavy vehicles. EMPA report No.220, Dübendorf, 1992.
- [22] Kawatani M, Yamada Y, Kim CW, Kawaki H. Estimation of slab's response in traffic-induced vibration of highway bridge by three-dimensional analysis. Journal of Structural Engineering, JSCE 1998; 44A: 827-34. (in Japanese)
- [23] Sakano M, Mikami I, Miyagawa K. Simultaneous loading effect of plural vehicles on fatigue damages of highway bridges. In: Thoft-Christensen P, Ishikawa H, Editors. Reliability and optimization of structural systems V. IFIP Transactions B-12. Elsevier Science Publishes; 1993, p.221-28,
- [24] Dodds CJ, Robson MM. The description of road surface roughness. Sound and Vibrations 1973; 31(2):175-83.
- [25] Honda H, Kajikawa Y, Kobori T. Spectra of road surface roughness on bridges. Structural Division, ASCE 1982; 108(ST9):1956-66.
- [26] ISO 8606. Mechanical vibration-road surface profiles-reporting of measured data, ISO, 1995.
- [27] Honda H, Kajikawa Y, Kobori T. Roughness characteristics at expansion joint on highway bridges, Proceedings of JSCE 1982; (328):173-76. (in Japanese)
- [28] Hanshin Expressway Management Technology Center (HEPC). Crack damage of RC deck slabs of highway bridges and its resistance, 1991. (in Japanese)
- [29] Okada K, Okamura H, Sonoda K, Fatigue failure mechanism of reinforced concrete deck slabs, TRB, Transportation research record 1978; 664:136-44.
- [30] Matsui S and Muto K, Rating of lifetime of a damaged RC slab and replacement by steel plate-concrete composite deck. Technology Reports of the Osaka University 1992; 42(2115): 329-40.
- [31] Perdikaris PC, Petrou MF, and Wang A (1993), Fatigue strength and stiffness of reinforced concrete bridge decks, Final report to ODOT, FHWA/OH-93/016, March 1993, Department of Civil Engineering, Case Western University, Cleveland, OH.
- [32] Maeda Y, Matsui S. Punching shear load equation of reinforced concrete slabs, Proceedings of JSCE 1984; (348)/V-1:133-41. (in Japanese)

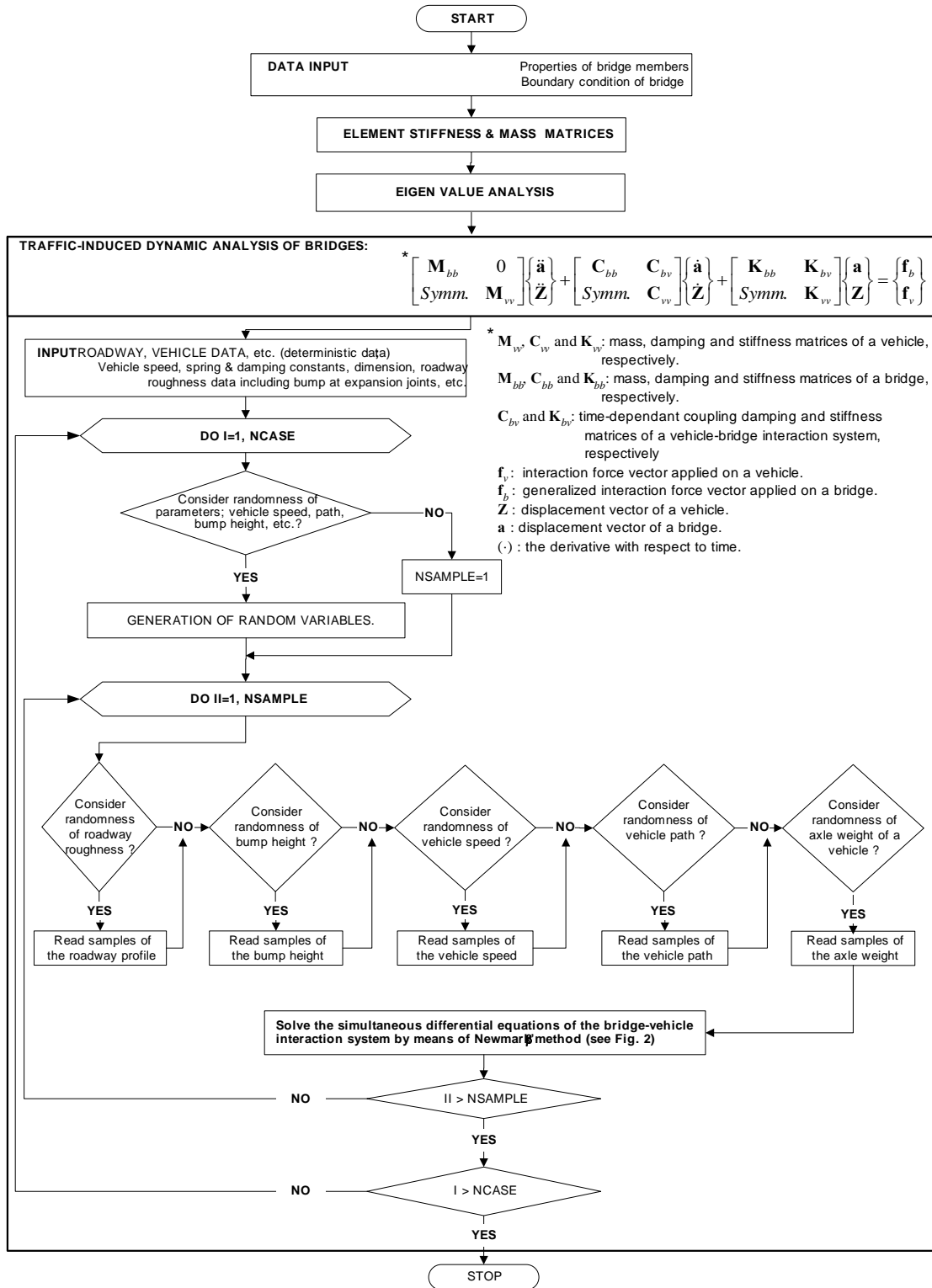


Fig. 1. Analytical procedure.

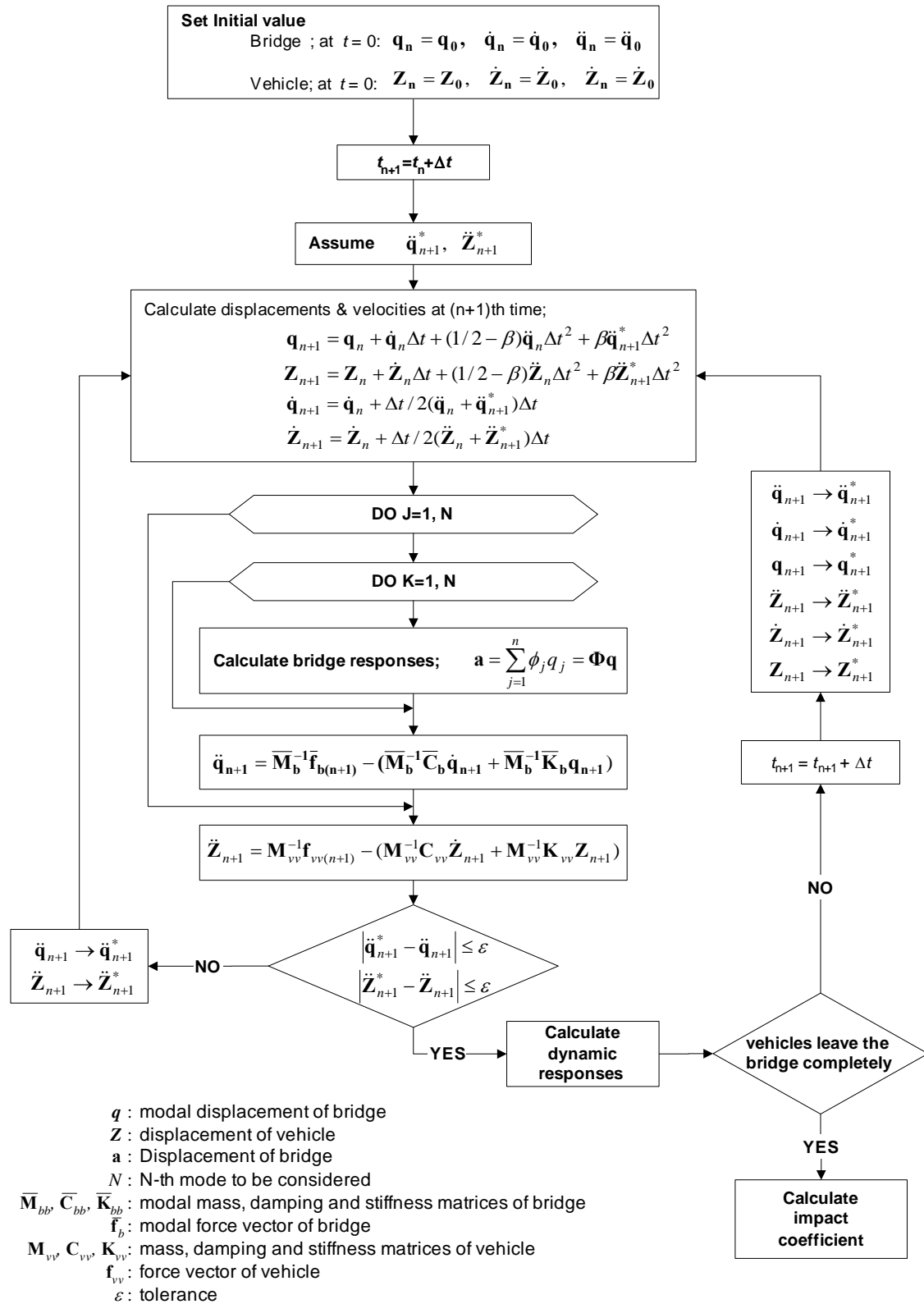


Fig. 2. Iterative process by Newmark's β method.

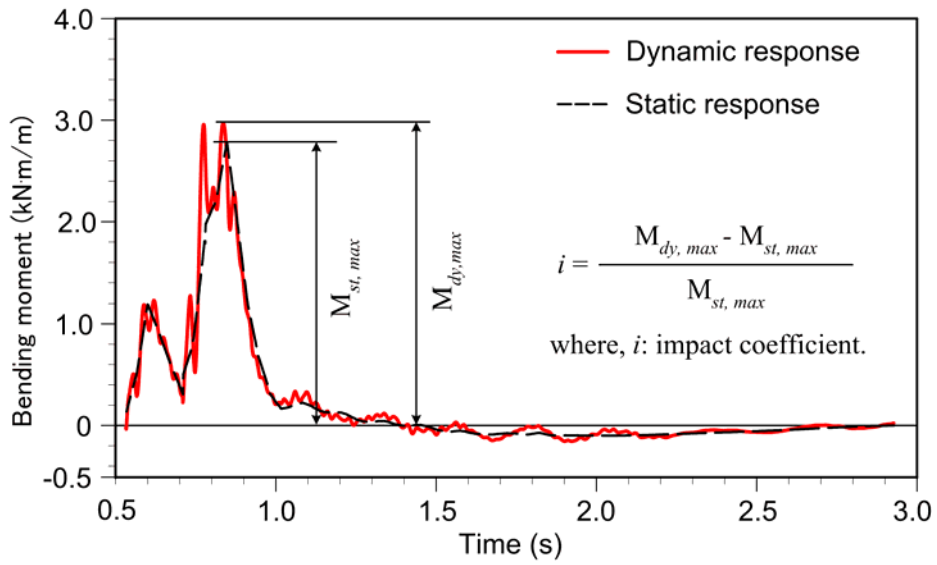


Fig. 3. Definition of impact coefficient.

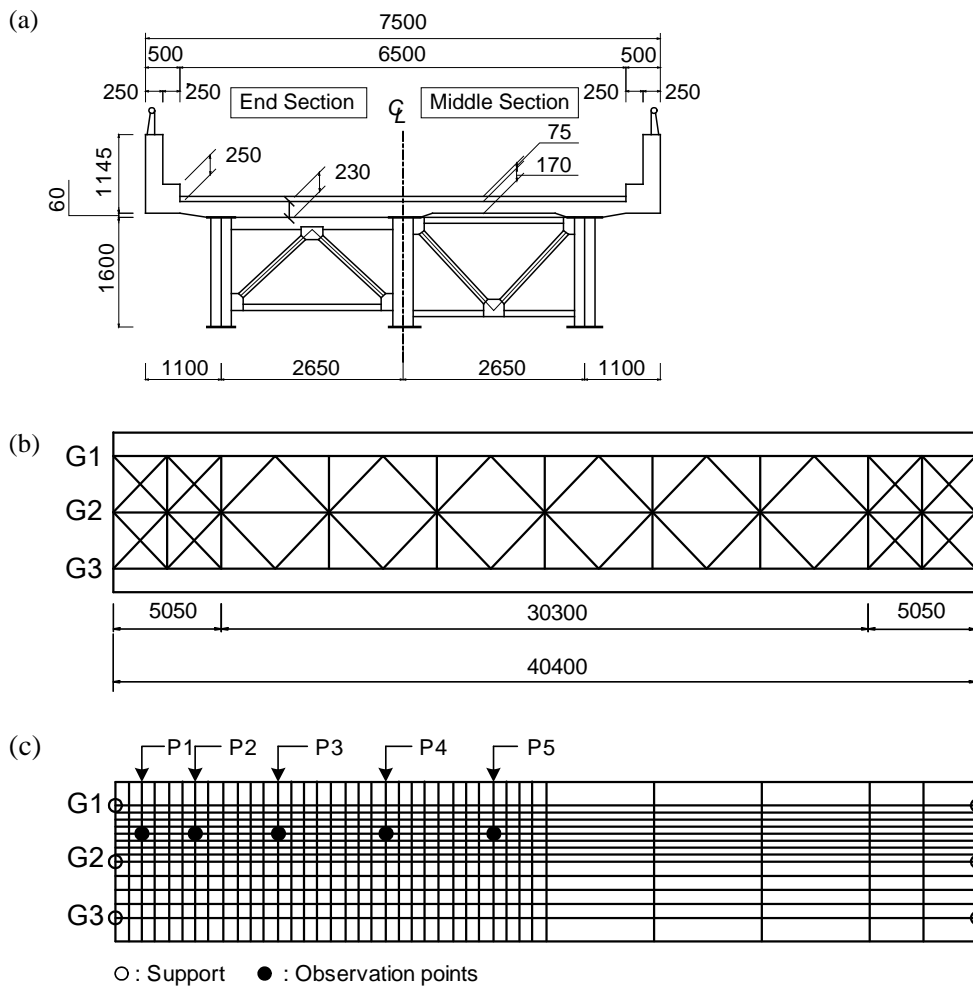


Fig. 4. Simply supported steel plate girder bridge with RC deck (unit: mm). (a) Cross sectional view, (b) Plan view, (c) FE model.

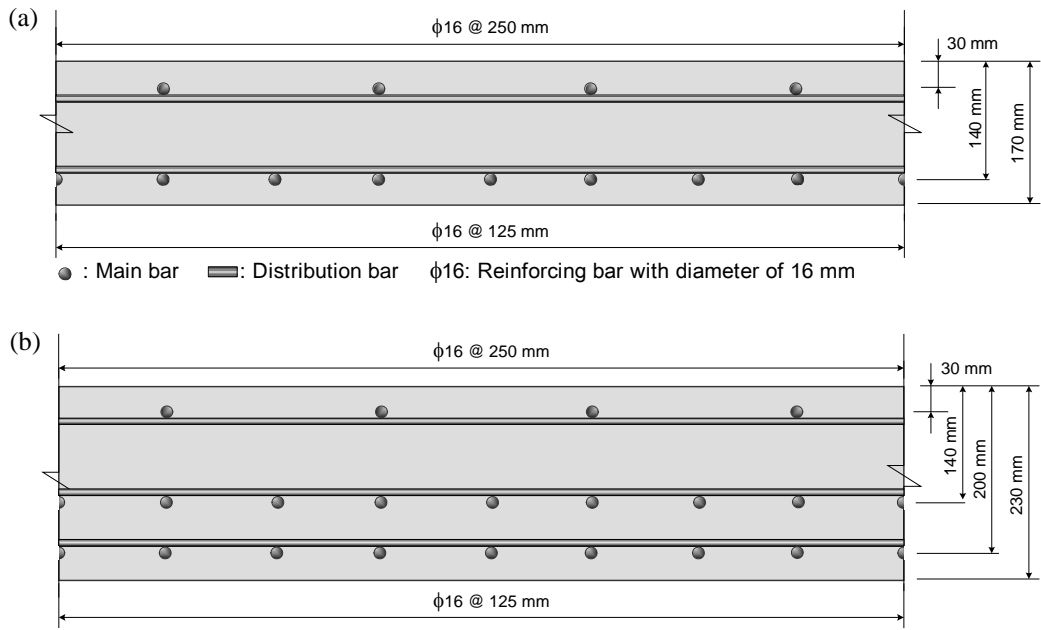


Fig. 5. Cross-section of RC slabs. (a) Middle-section, (b) End-section.

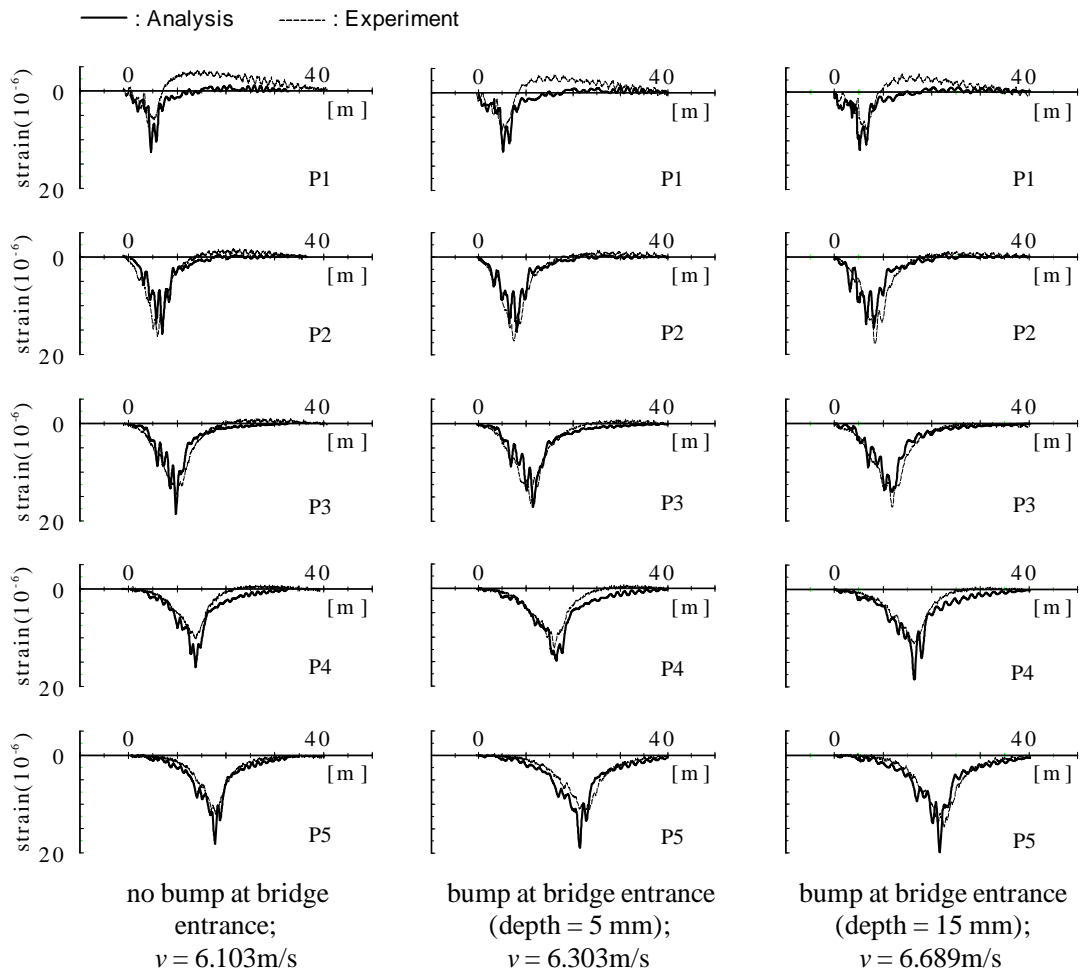


Fig. 6. Time histories of deck slabs taken from experiment and analysis.

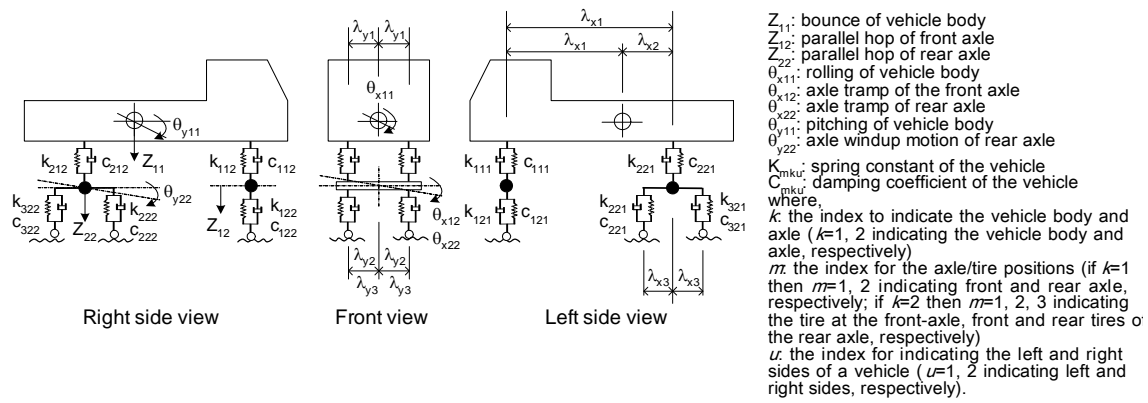


Fig. 7. Three-axle dump truck model with 8 DOFs.

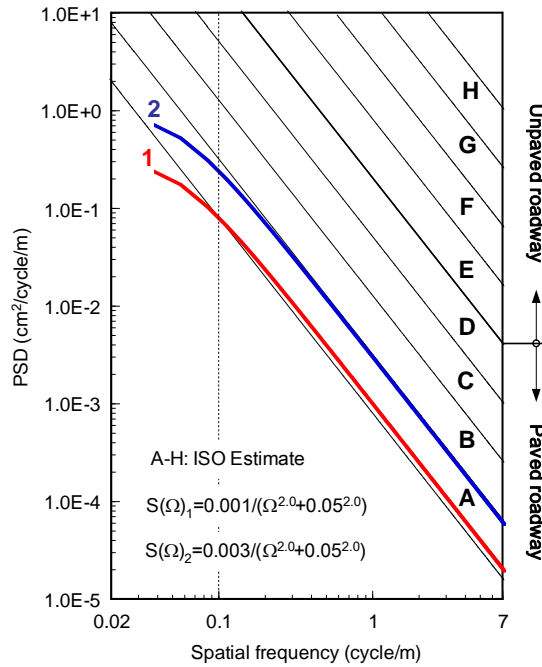


Fig. 8. PSD curves of roadway roughness model.

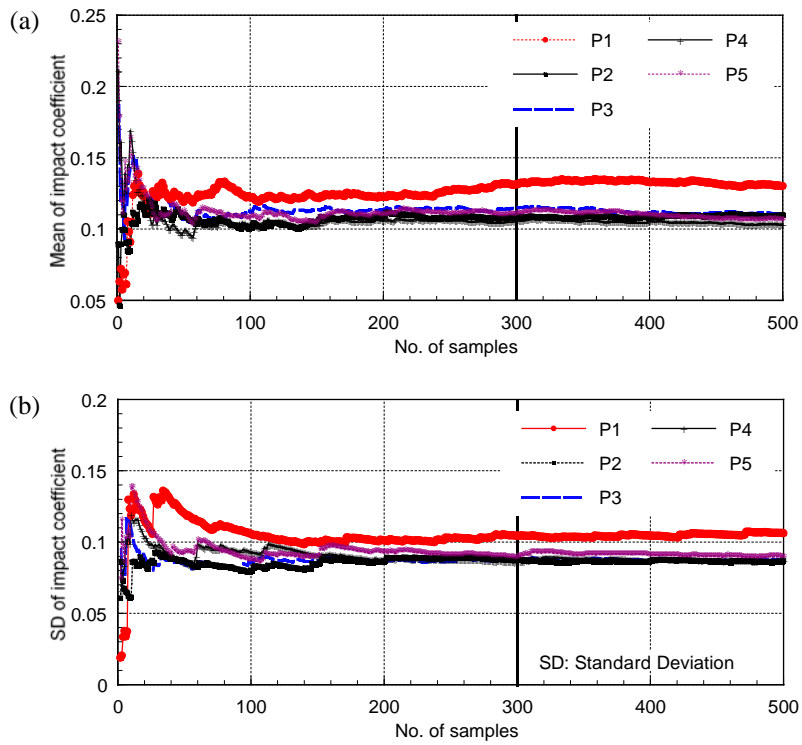


Fig. 9. Convergence of the simulated impact coefficients according to the number of samples (SCN-1). (a) Mean value, (b) Standard deviation value.

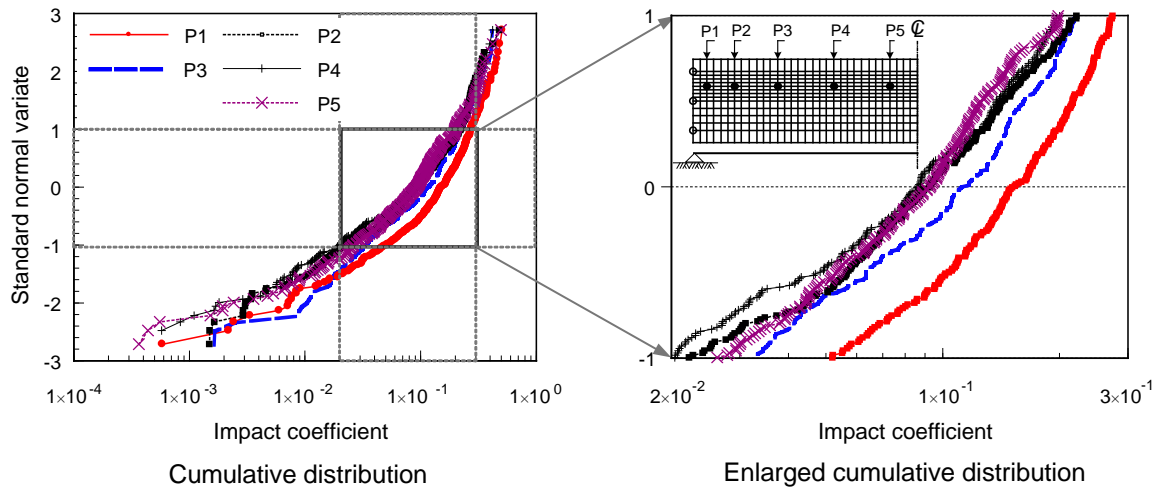


Fig. 10. Cumulative distribution of simulated impact coefficients of RC decks, considering all the random variables in MCS (SCN-1).

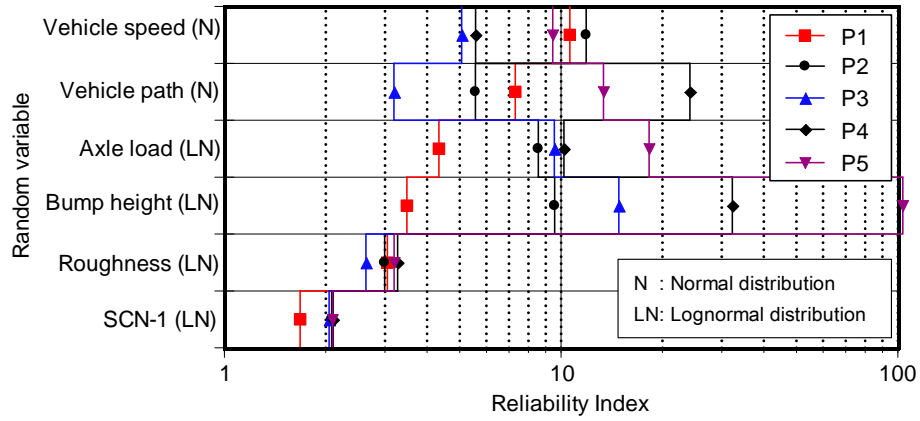


Fig. 11. Effect of random variable on reliability index of the impact coefficients specified in JRA code.

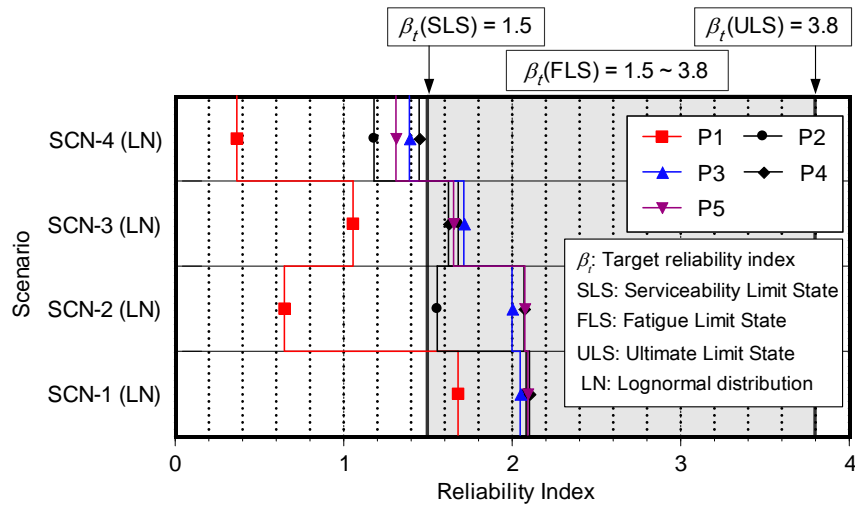


Fig. 12. Effect of each scenario on reliability index of the impact coefficients specified in JRA code.

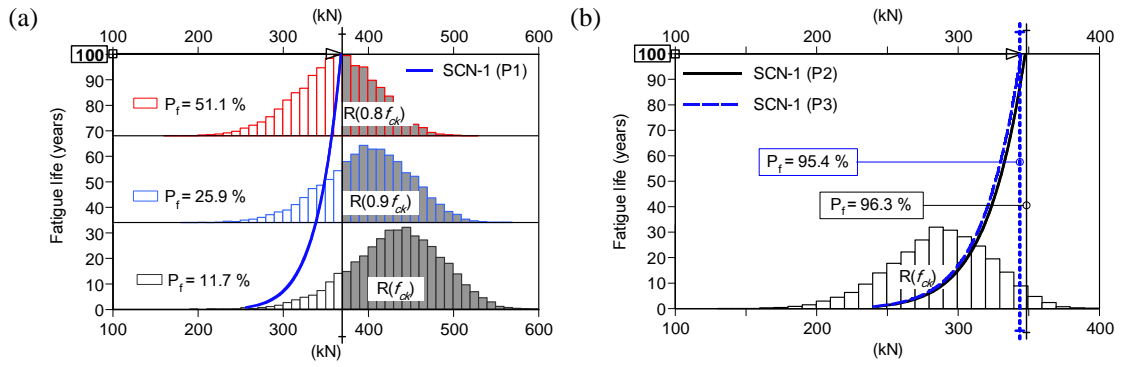


Fig. 13. Fatigue life of RC decks (SCN-1). (a) P1 panel, (b) P2 and P3 panels.

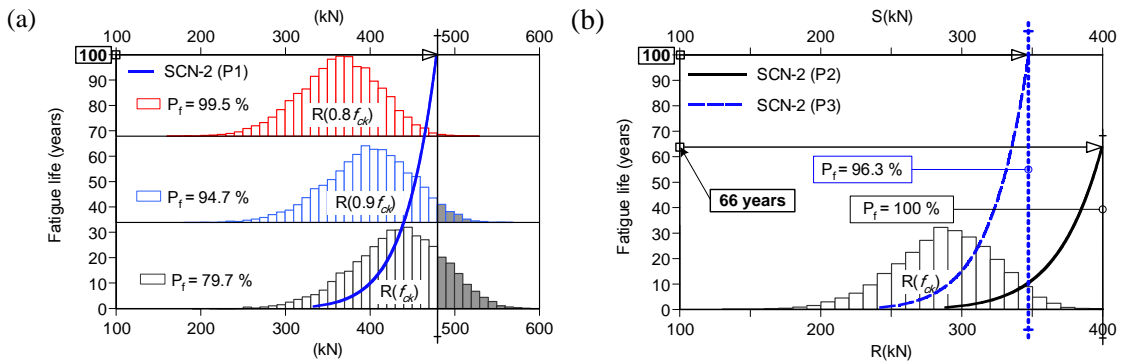


Fig. 14. Fatigue life of RC decks (SCN-2). (a) P1 panel, (b) P2 and P3 panels.

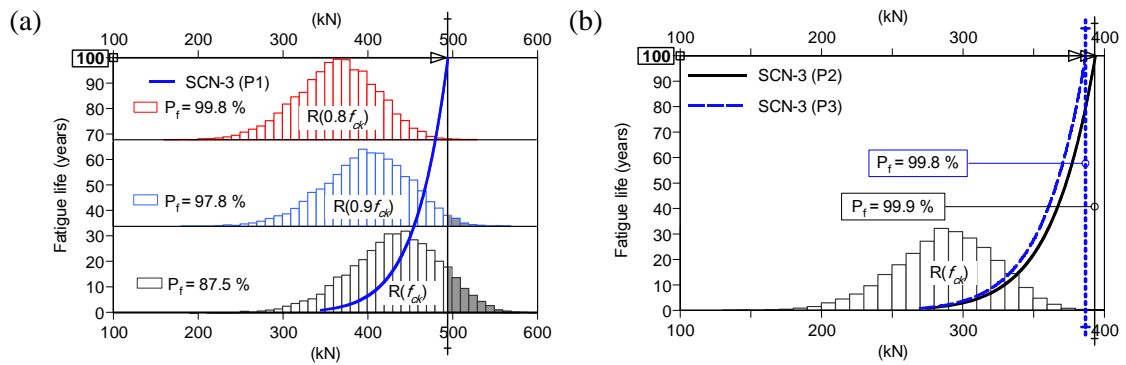


Fig. 15. Fatigue life of RC decks (SCN-3). (a) P1 panel, (b) P2 and P3 panels.

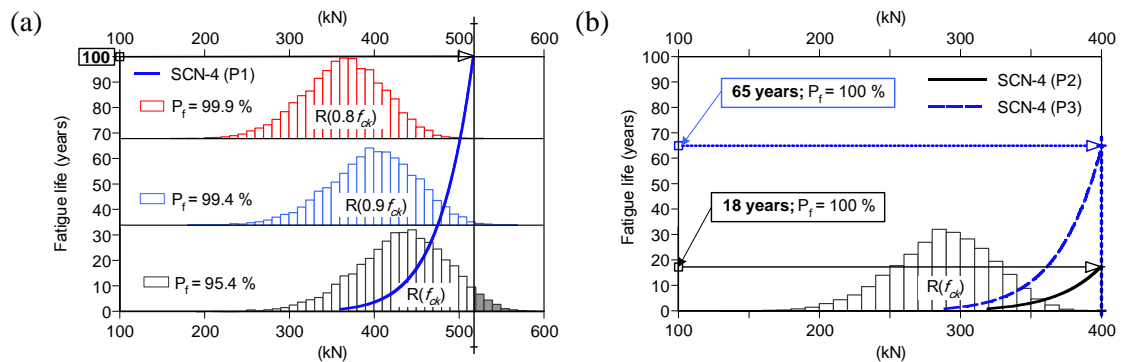


Fig. 16. Fatigue life of RC decks (SCN-4). (a) P1 panel, (b) P2 and P3 panels.

Table 1
Steel bridge properties

Mass per unit length (ton/m)		7.550
Section area of girders (m ²)		0.142
Moment of inertia (m ⁴)		0.212
Torsional constant (m ⁴)		0.0548
Damping constant (1 st and 2 nd modes)		0.0254
Fundamental natural frequency (Hz)	1 st (Bending)	2.34
	2 nd (Torsion)	3.81

Table 2
Vehicle properties

Parameters		Three-axle dump truck
Geometry (m)	Tread	1.80
	Distance between front and rear axle	3.99
	Distance of tandem axle	1.32
	Distance between front axle and CG	2.99
Weight (kN)	Gross	191.00
	Sprung mass including payload	171.40
	Steer axle unsprung mass	4.90
	Drive axle unsprung mass	14.70
Damping constant	Sprung mass (suspension)	0.03
	Unsprung mass (tire)	0.17
Fundamental frequency (Hz)	Bounce	3.30
	Axle hop	17.90

※ CG: Center of Gravity

Table 3
Impact coefficients taken from simulation

Scenario	Panel	P1 Mean (SD)*	P2 Mean (SD)	P3 Mean (SD)	P4 Mean (SD)	P5 Mean (SD)	G1 Mean (SD)
SCN-1		0.168 (0.1083)	0.114 (0.0895)	0.126 (0.0894)	0.108 (0.0895)	0.110 (0.0897)	0.049 (0.0352)
SCN-2		0.309 (0.1860)	0.163 (0.1309)	0.133 (0.0920)	0.111 (0.0914)	0.112 (0.0907)	0.049 (0.0357)
SCN-3		0.227 (0.2033)	0.150 (0.1193)	0.147 (0.1157)	0.156 (0.1236)	0.152 (0.1218)	0.084 (0.0550)
SCN-4		0.361 (0.2122)	0.216 (0.1615)	0.191 (0.1369)	0.184 (0.1321)	0.195 (0.1525)	0.087 (0.0546)

SCN-1: $S(\Omega) = 0.001/(\Omega^{2.0} + 0.05^{2.0})$; $v(\text{mean, SD}) = (70, 10)$ km/h; bump(mean, SD)=(10.2, 3.5) mm
SCN-2: $S(\Omega) = 0.001/(\Omega^{2.0} + 0.05^{2.0})$; $v(\text{mean, SD}) = (70, 10)$ km/h; bump(mean, SD)=(20.4, 7.0) mm
SCN-3: $S(\Omega) = 0.003/(\Omega^{2.0} + 0.05^{2.0})$; $v(\text{mean, SD}) = (50, 10)$ km/h; bump(mean, SD)=(20.4, 7.0) mm
SCN-4: $S(\Omega) = 0.003/(\Omega^{2.0} + 0.05^{2.0})$; $v(\text{mean, SD}) = (70, 10)$ km/h; bump(mean, SD)=(20.4, 7.0) mm
* SD means the Standard Deviation value.

Table 4
Properties of the RC deck

	Panel	Value
Concrete		
Compressive strength (f_{ck} ; MPa)		20.58
Normal (μ : 20.58, V : 0.165)		
μ : mean, V : coefficient of variation		
Young's modulus (MPa)		230300.0
Slab thickness (cm)	P1	23.0
	P2-P5	17.0
Reinforcing steel		
Yield strength (f_y ; MPa)		295.0
Young's modulus (MPa)		2058000.0